JOURNAL OF MATERIALS SCIENCE 20 (1985) 578–584

Shape accommodation during grain growth in the presence of a liquid phase

W. A. KAYSSER, M. ŽIVKOVIĆ*, G. PETZOW
Max-Planck-Institut für Metallforschung Institut für Werkstoffwissenschaften Pulvermetallurgisches Laboratorium Heisenbergstr. 5, 7000 Stuttgart 80, West Germany

The shape change of large tungsten spheres in a matrix of small tungsten particles and nickel-rich melt was studied. The formation of polyhedral particle shapes, which require less interspace to be filled with melt or pores may be caused by shape accommodation or contact flattening. Calculations support that shape accommodation during Ostwald ripening occurs, due to the small cross sections for diffusion in the melt of the neck areas of the large growing particles. It was shown that shape changes caused by shape accommodation may occur even at low stresses in flat neck areas in contrast to the contact flattening mechanism which require high stresses in these regions.

1. Introduction

During liquid-phase sintering of systems where components constituting the solid particles have a certain solubility in the melt, grain growth and shrinkage are two phenomena which were often found to occur simultaneously. From experiments with mixtures of large (225 μm) and small (10 μm) tungsten powders annealed in the presence of nickel-rich melt, Yoon and Huppmann [1, 2] set forth the idea that shrinkage is directly linked to grain growth. During prolonged liquid-phase sintering the small (10 μm) tungsten particles partially dissolved and solid phase precipitated on to the large (225 μm) single crystal spheres (Figs. 1a to d). The initial spherical shape of the large tungsten particles changed towards polyhedral shapes (with roundish edges and corners) by the reprecipitating material, wherever large particles were in an intimate vicinity. At the same time, the number and volume fraction of small particles was decreasing due to coarsening in the set of small particles and due to material losses to the large tungsten spheres. The shape change of the large tungsten spheres may have resulted from spherical growth due to Ostwald ripening and subsequent contact flattening when large spheres came into contact with other large spheres. Alternatively the shape change may be due to Ostwald ripening in a "shape accommodating" way.

From Fig. 1b (arrow), it is evident that the virtual "contact flattening" should be a fast process which acts on spheres of a virtual diameter of 225 μm during liquid-phase sintering at 1680° C for 30 min to give flattened areas which are 90 to 150 μm wide. Spheres which are in direct contact initially, were thus expected to reveal considerable contact flattening, i.e. should change to partially truncated spheres where parts of the initial spheres are cut off. Fig. 1c shows that the virtual contact flattening never induced the truncation of the initial spheres, although wide flat areas were found where large spheres were in intimate contact. These observations support that contact flattening, which was proposed by Kingery [3], is of minor influence for these large particles and that those large particles were growing in a shape accommodating way.

It is the purpose of this paper to show by simple calculations that shape change towards an improved shape accommodation may be caused by geometrical conditions in the neck areas of large growing particles, without the necessity of simultaneous contact flattening.

*On leave from Računski Centre, Institute Boris Kidrič, Vinča, Beograd, Yugoslavia.

0022–2461/85 $03.00 + .12

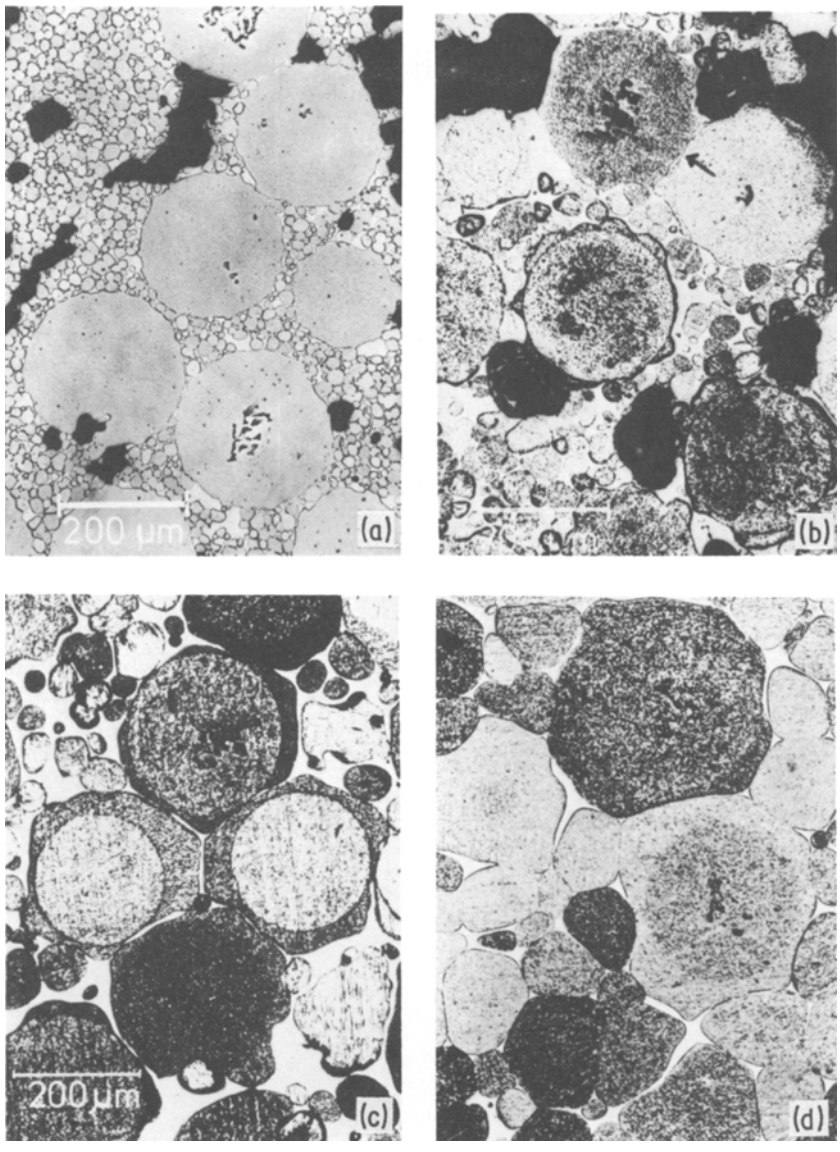

Figure 1 Microstructure of a mixture of fine (10 µm) and large (225 µm) tungsten particles after liquid-phase sintering in the presence of nickel at 1680° C, (a) for 3 min; (b) for 30 min; (c) for 120 min; (d) for 360 min.

2. Model and assumptions

Figs. 2a and b shows the initial and later geometric arrangement used for the calculations. Three large spheres of radius R_0, which include an angle β, are immersed in a "matrix" of much smaller particles of the same material and a certain amount of liquid phase (grey). The liquid phase serves as a fast transport medium and is present in the contact areas of the large particles as a thin liquid film of thickness, δ. The transport via the melt during dissolution and reprecipitation is assumed to be diffusion-controlled [4, 5]. The set of small particles is coarsened by diffusion-controlled Ostwald ripening. The average concentration of solute in the melt will be above the equilibrium concentration which would result from a flat solid/liquid interface. The increased solute concentration in the melt will lead to a diffusion-controlled deposition of material on the large particles as long as the curvature of the solid/liquid interfaces of the large particles is smaller than (appr.) the average curvature of the small particles. Deposition may occur on all interface sites of the large spheres. Some constraints are shown in Fig.

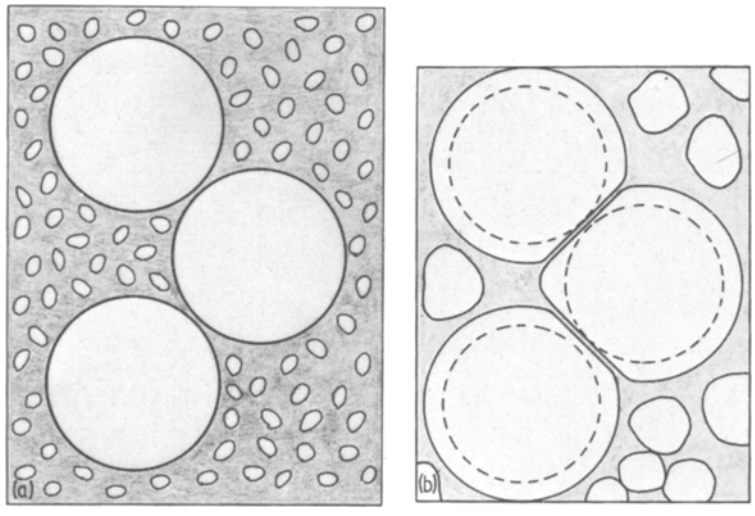

Figure 2 Geometric arrangement of large and small tungsten particles in nickel-rich melt before and after liquid-phase sintering. A pore providing a hydrostatic pressure on the arrangement is assumed to be present in the system elsewhere (grey = liquid phase). (a) Initial state. (b) After liquid-phase sintering.

2b. It is assumed that flat contact areas, CA, if they develop between the spheres, will be tangents to the interface (circular) with radius R_i. Any movement of the large particles is excluded, except those migrations which result from the deposition of additional material in the neck areas. No pressure in the contact area is assumed to exist beyond values which maintain the thickness δ of the liquid film.

Fig. 3 shows a detailed geometric description of the contact area between the two initially spherical particles I and II. At first the geometry is equal to the section shown in Fig. 2a. From dissolving small particles, material is reprecipitated on to the large particles. The growth rate of particle I at the area near to Z is determined by the curvatures $2/R_{i-1}$ and $2/\bar{r}$. After growing for a small time interval, Δt_i, the liquid solid interface Z is assumed to have shifted from position U_{i-1} to position U_i by the finite distance $\Delta U_i = U_i - U_{i-1}$. A new radius of the curved interface R_i^+ at Z is found by the condition of being a circle with its centre on line L, intersecting line L in Z, and having the virtual extension of the flat contact area between particles I and II as a tangent. This circle determines the new size of the contact area, a_i^+. Material

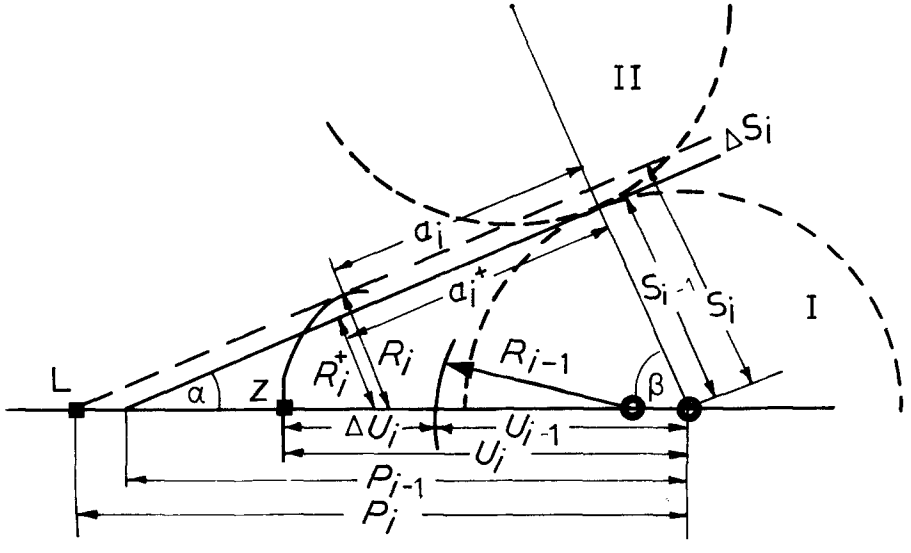

Figure 3 Geometry for calculation.

deposited in the contact area (CA with radius a_i^+) during the time interval, Δt_i, will lead to a migration of the liquid/solid interface in the contact area by ΔS_i. The contact area in the new position S_i is then virtually extended to form a tangent to a circle of radius R_i with its centre on line L and its section of line L in the new position of Z. Radius R_i is taken as new radius of curvature at Z. The calculation then proceeds for a subsequent time interval Δt_{i+1}.

In a short time interval, Δt_i, the solid/liquid interface is assumed to shift from position U_{i-1} to U_i by $\Delta U_i = U_i - U_{i-1}$. According to Zener [5] and Carslaw and Jaeger [6] we obtain

$$\Delta U_i = \Delta t_i D \Gamma \left[\left(\frac{1}{\bar{r}_i} \right)^2 - \left(\frac{1}{R_{i-1}} \right)^2 \right], \quad (1)$$

where $\bar{r}_i$ is the average particle radius of the set of small particles, R_{i-1} is the radius of curvature of the large particle at the growing area, D is the diffusion coefficient in the liquid. The constant Γ is given by

$$\Gamma = \frac{2\gamma_{SL}\Omega C_0}{RT}, \quad (2)$$

where γ_{SL} is the specific interface energy liquid/solid, Ω is the molar volume, R is the gas constant and T the absolute temperature. C_0 is the solubility of a solute in the liquid in the case of a flat interface solid/liquid and will be given in m^3 m^{-3}.* Thus Γ has the units m. This average radius of the set of small particles will be calculated by

$$\bar{r}_i = (\bar{r}_0^3 + kt_i)^{1/3}, \quad (3)$$

assuming a growth law, valid for diffusion controlled Ostwald ripening [4], where $\bar{r}_0$ is the initial average particle radius of the set of small particles, t_i is the effective annealing time ($t_i = t_{i-1} + \Delta t_i$) and k is a growth constant with the units $m\,sec^{-1}$.

From ΔU_i and the geometrical constraints, the parameters R_i^+ and a_i^+, shown in Fig. 3, can be calculated (for details of the numerical calculation see the Appendix).

The material flowing into the cylindrical thin liquid disc with height δ and radius a_i in a time interval Δt_i is given by (compare with [6])

$$\Delta J_i = 4\pi D \delta \Delta C_i \Delta t_i, \quad (4)$$

and with ΔC_i in $m^3\,m^{-3}$,

$$\Delta J_i = \Delta V_i \quad (5)$$

yielding†

$$\Delta S_i = \frac{\Delta V_i}{2\pi (a_i^+)^2} \quad (6)$$

with (Thomson–Freundlich)

$$\Delta C_i = C_0 \frac{\Omega \gamma_{SL}}{RT} \frac{1}{R_i^+}, \quad (6)$$

ΔC_i is the difference of the concentration of element, i, in the melt near the interface with radius R_i^+ and near the flat interface in the contact area. The units of ΔC_i are again $m^3\,m^{-3}$. The sequence of steps for the numerical calculation are shown in the Appendix.

3. Results and discussion

The shape change calculated with the data $D = 4.5 \times 10^{-9}\ m^2\ sec^{-1}$, $\gamma_{LS} = 0.35\ J\,m^{-2}$, $C_0 = 0.4$, $R_G = 8.31\ J\,mol^{-1}\,K^{-1}$, $T = 1953\,K$, $k = 0.7 \times 10^{-18}\ m^3\,sec^{-1}$ [6] $\Omega = 9.53 \times 10^{-5}\ m^3\,mol^{-1}$, $\delta = 10^{-6}$ m, $\bar{r}_0 = 5 \times 10^{-6}$ m, $\bar{R}_0 = 10^{-4}$ m, $d = 45°$, and $a_0 = 10^{-6}$ m is shown in Fig. 4. At first it is interesting to note that the deposition of material in the contact area is extremely small, i.e. the distance between the particle centres remains essentially constant. This result is in accordance with the observation that large spheres in direct contact after short liquid-phase sintering, show considerable shape accommodation resulting from material deposited on to the spheres (Fig. 1b, arrow), but only negligible deposition in the contact area. The shape accommodation, i.e. the deviation from the spherical shape thus seems to be due to the low deposition rate in the contact area which results from the low material flow rate in the thin liquid layer.

Independent of this general conclusion, the analysis of the sequence in Figs. 1a to d and of the calculations, provides some interesting results. Shape accommodation after 2 h (Fig. 1c) reveals

*Equation 1 and this step are only correct, if $c_j^S \gg \Sigma_{m=1}^{n} c_m^S$.

†D, C_0 and Ω are taken for that element, j, which has the lowest value of $[D_j \cdot (C_{j0}^L / C_j^S) \cdot \Omega_j \cdot \Sigma_{m=1}^{n} c_m^S]$ where C_{j0}^L is the solubility of element j, if the liquid is in contact with solid solution by a flat interface liquid/solid. n is the number of components, m is an index, c_j^S is the solubility of element j in the solid solution, c_m^S are the solubilities of other elements in the solid solution. Ω_j and D_j are the molar volume and the diffusion coefficient in the liquid of elements j, respectively.

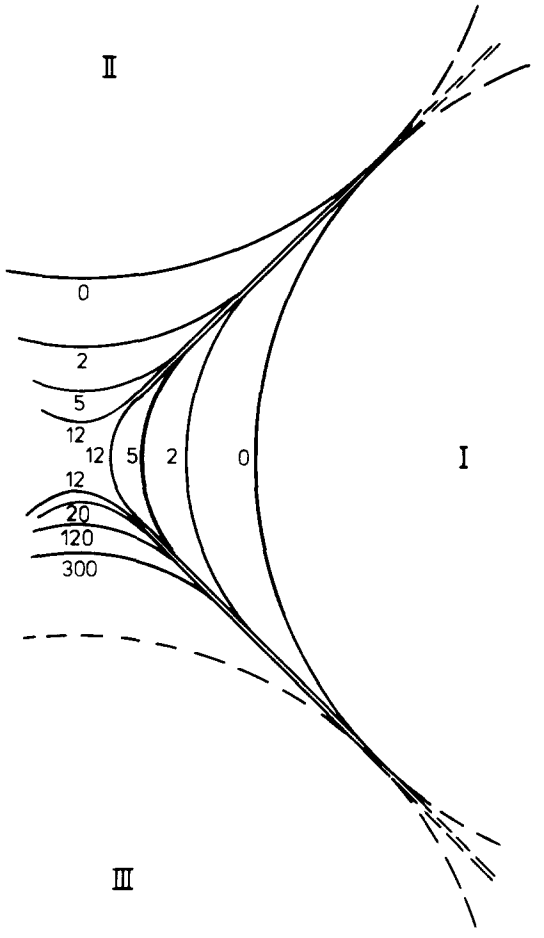

Figure 4 Shape accommodation during liquid-phase sintering (calculated). Grains I and II show the shape change during the initial 12 min of sintering. Grain III shows the shape change in the time interval between 12 and 300 min.

interface areas of higher convex curvature in the shape-accommodated area than after longer liquid-phase sintering (6 h, Fig. 1d). In respect of the calculations this would mean a change in the shifting direction of the liquid/solid interface, i.e. a decrease of U_i with time. Fig. 5 shows this effect to arise in the calculations when $\bar{r}_i$ becomes larger than R_{i-1}. This would indicate a direct relation between the average curvature of the set of small particles and the highest curvature which could be developed by shape accommodation. The average curvature of the interface areas connecting flat contact regions in shape-accommodated microstructure areas after sintering at 1680° C for 2 h shown in Fig. 1c, is $6.66 \times 10^{-2}\ \mu m^{-1}$. The distribution of curvatures shows frequency maxima at $5 \times 10^{-2}\ \mu m^{-1}$ and $1.1 \times 10^{-1}\ \mu m^{-1}$ which may correspond to the typical curvature along edges and at corners of the large polyhedrons, respectively. The lower frequency maximum has to be compared with the curvature of the average particle $7.9 \times 10^{-2}\ \mu m^{-1}$. After sintering at 1680° C for 6 h the corresponding data are 3.75×10^{-2}, 2.56×10^{-2} and $5.88 \times 10^{-2}\ \mu m^{-1}$ for the average curvature, the upper and lower frequency maxima of the shape-accommodation area and $4.4 \times 10^{-2}\ \mu m^{-1}$ for curvature of the average small particle. After both annealing times the average particle size yields a curvature which is slightly above the average curvature of the growing particles. The fragmentary set of data does not allow us to draw a final conclusion‡ but, nevertheless, it supports a shape-accommodation mechanism where small particles dissolve and reprecipitate rapidly on to large particles, as long as the interface liquid/solid of the small particles has a much higher curvature than the interface connecting contact regions of the large particles.

Many of the large particles show that considerable amounts of material are also deposited in contact areas (Fig. 1c). The deposition of material in the contact regions may be caused by various material flows or their combinations. Fig. 6 shows schematically the microstructural changes expected from (a) deposition by radial flow inwards, as calculated above, (b) deposition by perpendicular flow to the larger particle on the left-hand side, (c) combination of perpendicular flow of the left and radial inward flow, (d) combination of perpendicular flow to the left and radial outward flow. Dissolution of very small particles near to very large particles may result in a shape shown in Fig. 6a. The latter mechanism seems to be important in the sintering stage shown in Fig. 1b. When dissolving and growing particles are of the same order of size, the mechanisms shown in Figs. 6b to d will become more and more dominant. It is thus not possible to conclude unambiguously from the observation of shape accommodation at large spheres in the presence of small particles, that the same mechanism must dominate shape changes during coarsening of a set of small particles with a usual particle size distribution, e.g. narrow log-normal. The mathematical treatment of a narrow distribution is less simple than the numerical calculation conducted earlier in this

‡Other explanations would be related to the capillary pressure in the presence of pores.

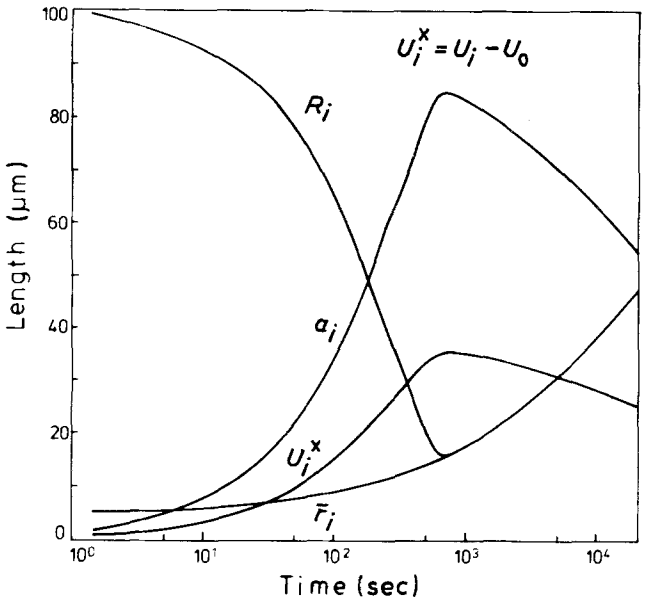

Figure 5 Development of $\bar{r}_i$, U_i^x, a_i and R_i (see text) during liquid-phase sintering of W–Ni (calculated).

paper and will be attempted in a further work.

4. Conclusions

Shape accommodation of large single-crystal tungsten spheres in the presence of small tungsten particles and nickel-rich melt can be shown to be due to dissolution of small particles and the reprecipitation on to the large sphere. Calculations support the assumption that the deposition rate in flat contact areas of adjacent large particles is very small, compared to the deposition rate at areas where the liquid/solid interfaces of larger particles are further apart. A straight conclusion to an equivalent shape-accommodation mechanism in a set of particles with a narrow size distribution seems unjustified.

Acknowledgement

This work was performed under a joint research programme between the Deutsche Forschungsgemeinschaft (DFG, Pe-205/1) and the Korea Science and Engineering Foundations (KOSEF). Part of this work was done when one of the authors (WAK) was guest scientist at Massachusetts Institute of Technology, Cambridge, Mass., USA. M. Živković thanks the International Bureau of KFA-Jülich for financial support.

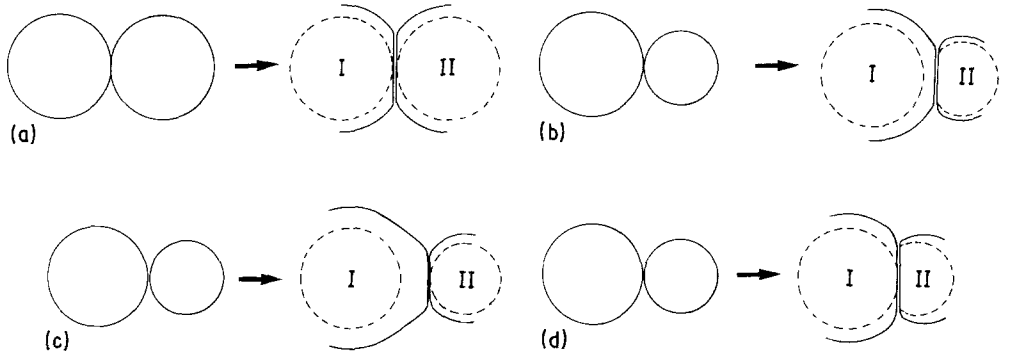

Figure 6 Grain growth and shape change during liquid-phase sintering (schematic). The size of the average particle is assumed to be smaller than the particles shown in (a) to (d). (a) Equal deposition on the both particles I and II. This case was assumed for the calculations. (b) Deposition on to particle I is faster than on to particle II. Particle I grows at the expense of particle II (directed growth). (c) Deposition on to particle I is faster than on to particle II. Directed growth and slow contact flattening. (d) Simultaneous deposition and contact flattening. Contact flattening is faster than deposition and directed flow.

Appendix

The sequence of numerical calculation steps starts with Equation 4 using R_{i-1} and $\bar{r}_i$. A new R_i, a_i and P_i are then calculated by

$$R_i^+ = (P_{i-1} - U_i)\left(\frac{\sin\alpha}{1-\sin\alpha}\right) \quad \text{(A1)}$$

$$a_i^+ = (U_i - R_i^+)\cos\alpha \quad \text{(A2)}$$

$$\Delta S_i = \frac{2D\delta\Gamma\Delta t_i}{(a_i^+)^2 R_i^+} \quad \text{(A3)}$$

$$S_i = S_{i-1} + \Delta S_i \quad \text{(A4)}$$

$$P_i = \frac{S_i}{\sin\alpha} \quad \text{(A5)}$$

$$R_i = (P_i - U_i)\left(\frac{\sin\alpha}{1-\sin\alpha}\right) \quad \text{(A6)}$$

$$a_i = (U_i - R_i)\cos\alpha. \quad \text{(A7)}$$

References

1. D. N. YOON and W. J. HUPPMANN in "Contemporary Inorganic Materials 1978", edited by G. Petzow and W. J. Huppmann (Dr. Riederer-Verlag, Stuttgart, 1978) p. 55.
2. *Idem, Acta Metall.* **27** (1979) 693.
3. W. D. KINGERY, *J. Appl. Phys.* **20** (1959) 301.
4. C. WAGNER, *Z. Elektrochemie* **65** (1961) 581.
5. C. ZENER, *J. Appl. Phys.* **20** (1949) 950.
6. H. S. CARSLAW and G. C. JAEGER, "Conduction of Heat in Solids", (Clarendon Press, Oxford, 1947).

Received 27 January
and accepted 10 April 1984